Chapter 11
Graphene Quantum Dots in Various Many-Electron π-Models

Anatoliy Luzanov

11.1 Introduction

After the discovery of graphene, there has been a rising interest in its fundamental electronic properties. Up to now, graphene nanoparticles, in particular graphene quantum dots (GQDs), remain an extremely important topics in solid-state physics and material sciences [1–5]. There are many useful models and techniques for studying GQD electronic structure, and among them are the conventional tight-binding (TB) model and its Hückel version for π-electron shells. Certainly, simple Hückel and TB computations provided many important results for understanding the unique physics of graphene systems (e.g., see [2]). At the same time, accounting for many-electron effects is essential in this case of extended delocalized systems containing a lot of conjugated bonds.

The present work continues our previous study on the electronic structure of carbon-containing nanoclusters [6–11]. One of the principal aims of this paper is to show that some well-known quantum chemistry models which are less familiar to the graphene research community can be served as a suitable and feasible tool for exploring nanographenes at the semiempirical many-electron level. In particular, we apply here the so-called spin-extended Hartree-Fock (EHF) and restricted active space configuration interaction (RAS-CI) methods.

Another goal of the work is to elucidate, for the selected graphene-like molecules, a behavior of π-electrons in extreme electric fields. In this problem, the electron unpairing (see review [8]) is a particularly exciting issue. At last, the problem of

A. Luzanov (✉)
State Scientific Institution "Institute of Single Crystals", National Academy of Sciences of Ukraine, Kharkiv, Ukraine
e-mail: luzanov@xray.isc.kharkov.com

O. Fesenko, L. Yatsenko (eds.), *Nanooptics, Nanophotonics, Nanostructures, and Their Applications*, Springer Proceedings in Physics 210,
https://doi.org/10.1007/978-3-319-91083-3_11

graphene aromaticity continues to attract interest [1, 12–14], and here we will also focus on it using the previously given approach [15] .

11.2 Computational Schemes

11.2.1 Electronic Instabilities and Lowest Excitations

In this and next subsections, we shortly sketch the main electronic models that we apply to GQDs. First, we consider rather qualitative schemes. Usually, the frontier orbital energy gap (the so-called HOMO-LUMO gap) is considered as a descriptor of the molecular stability. But this electronic indicator is too crude. More correct and more informative is the Hartree-Fock (HF) stability theory [16] (see also [17], Sect 10.10). We recall that the HF stability of the given molecular system means that the HF stability matrix (matrix of second derivatives with respect to variational parameters of HF wave function) has only positive eigenvalues λ^{stable}. An occurrence of zero or negative λ^{stable} values indicates on the HF instability of the system under study.

For closed-shell singlet states, the restricted HF (RHF) model is usually employed, and in this case one can define the Hartree-Fock stability of two types, singlet one and triplet one [16]. The corresponding eigenvalues of the HF stability matrix will be denoted by $\lambda^{\text{stable}}_{s=0}$ and $\lambda^{\text{stable}}_{s=1}$, respectively. Typically, minimum value of $\lambda^{\text{stable}}_{s=1}$ is lesser than minimum $\lambda^{\text{stable}}_{s=0}$, that is, the triplet RHF instability appears before the singlet HF instability does. In fact, the negative $\lambda^{\text{stable}}_{s=0}$ is an indicator of a very strong electronic instability. To be more specific, consider π-electrons in the hexacene molecule $C_{26}H_{24}$ for which we find $\lambda^{\text{stable}}_{s=1} = -1.16$ eV, and $\lambda^{\text{stable}}_{s=0} = 2.10$ eV (as for the π-parameterization adopted here see Sect. 11.3). We see that even this not so long oligocene structure is quite unstable and exhibits sufficiently strong electron correlation.

Along with the HF stability analysis, here we invoke typical models of lowest-energy electronic transitions. The simplest is the configuration interaction (CI) singles method, or CIS method. The corresponding minimal eigenvalues, $\lambda^{\text{CIS}}_{s=1}$ and $\lambda^{\text{CIS}}_{s=0}$, of the CIS Hamiltonian matrix give rather crude estimates of the lowest-energy singlet-triplet and singlet-singlet transitions. Considerably more advanced is the restricted active space CI (RAS-CI) method [17, 18]. In RAS-CI one divides the full one-electron orbital space into certain active and frozen orbital subsets. To deal with this, the standard full CI (FCI) technique is applied only to electrons assigned to the chosen active orbital subset. Then, the lowest eigenvalues of the appropriate RAS-CI matrix will approximate energies of the ground and excited states. For the low-lying excitation energies, the approach provides estimates more reliable than those from CIS.

In our study we employ a nonstandard but equivalent RAS-CI formulation. It is based on the many-electron equation describing a detachment of multi-electrons (say¸ 2 k electrons), from the intermediate state with $N + 2k$ electrons where $N \equiv 2n$ is a number of electrons in an even-electron molecule under study. Thus, we start with a polyanionic $(N + 2k)-$ electron state for which we form the Slater determinant

with $n + k$ occupied MOs. The aimed equation is the FCI eigenvalue problem for 2 k-electron Hamiltonian of the form

$$H^{\text{detach}} = -Q_{2k}^{\text{act}} \left[\sum_{1 \le i \le 2k} f(i) - \sum_{1 \le i < j \le 2k} g(i,j) \right] Q_{2k}^{\text{act}},$$

where f is the conventional Fock operator of the intermediate $2(n + k)$ electron singlet state (recall that $n = N/2$ is a number of electron pairs in the molecule under study); g is the two-electron Coulomb operator, and Q_{2k}^{act} is the 2 k-electron projection operator onto the chosen active subset. The lowest singlet-triplet, $\lambda_{s=1}^{\text{RAS-CI}}$, and singlet-singlet, $\lambda_{s=0}^{\text{RAS-CI}}$, excitation energies are evidently obtained from the corresponding differences of the H^{detach} eigenvalues. In practice, we carried out RAS-CI spectral calculations with $k = 6$. In terms of results, the computations are equivalent to those within the conventional RAS-CI 6 × 6 scheme. A lower part of the H^{detach} spectrum was computed by the modified Lanczos-type diagonalization algorithm described in Ref. [9], Appendix A.

11.2.2 Unrestricted and Extended Hartree-Fock Methods

Here the used HF schemes will be only briefly sketched. We begin with the unrestricted Hartree-Fock method (UHF) which is a precursor of EHF. The single-determinant UHF model is not accidentally named also as "spin-polarized Hartree-Fock method." Unlike RHF, the UHF method brings into play, if possible, spin-polarized MOs, i.e., different orbitals for different spins. The latter are usually signified by ϕ_j^{α} and by ϕ_j^{β} for spin-up and spin-down electrons, respectively. From these orbitals the fundamental projection operators, ρ^{α} and ρ^{β}, are constructed. In Dirac notation these are

$$\rho^{\alpha} = \sum_{1 \le j \le n+s} |\, \varphi_j^{\alpha} >< \varphi_j^{\alpha} \,|\,, \rho^{\beta} = \sum_{1 \le j \le n-s} |\, \varphi_j^{\beta} >< \varphi_j^{\beta} \,|\,,$$

and $n + s$ and $n - s$ are, respectively, total numbers of spin-up and spin-down electrons in the given N-electron state with a total spin s. By applying variational method, one can directly derive the conventional UHF equations in terms of ρ^{α} and ρ^{β} [19]. Although a certain correlation of opposite-spin electrons appears in the corresponding Slater determinant $|\Phi>$, the correlated state of this type does not exist in weakly correlated closed-shell systems. More exactly, in a such singlet-like case with $s = 0$, a nontrivial UHF solution is possible if the initial RHF singlet state satisfies the triplet Hartree-Fock instability condition, that is, $\lambda_{s=1}^{\text{stable}} < 0$ [20]. For strongly correlated systems (e.g., zigzag graphenes), the UHF model provides a more or less reasonable π-electron picture.

Now we proceed to the EHF approximation that was firstly formulated by Löwdin [21] for π-electron systems. There are many works on the EHF theory (see, e.g., reviews [22, 23]), and recently this theory was revived at the ab initio level [24]. In EHF the spin contamination of a trial UHF determinant |Φ> is removed by acting on |Φ> an appropriate spin-projection operator O_s. Generally, it depends on a spin z-projection value m as well. Thus, instead of |Φ>, we introduce the normalized EHF wave function as follows:

$$\left|\Phi^{\mathrm{EHF}}\right\rangle = O_s|\Phi\rangle/\sqrt{\langle\Phi|O_s|\Phi\rangle}.$$

It is important that, unlike UHF, the EHF theory imposes no restriction on electron correlation strength so that even for $s = 0$, the nontrivial EHF (i.e., $\phi_j^\alpha \neq \phi_j^\beta$) solution always exist [23]. This feature is very important for our aims because it allows us to treat weakly and strongly correlated problems on equal footing. Furthermore, there are many derivations and practical formulations of the EHF variational equations, but we prefer using matrix formulations in terms of ρ^α and ρ^β [23, 25], as they provide suitable and compact algorithms. Our matrix technique [25] is easily coded and applied to large molecules. At last, we must mention one essential drawback of EHF and related variational models (including half-projected HF and complex MO schemes). This is a lack of size consistency which precludes obtaining robust results for too large-scale systems.

11.3 π -Electron Properties of Selected Nanographenes

Now we will analyze the results of π-electron computations on small GQDs. For this study, we selected four rather typical honeycomb carbon structures which are similar in composition (Figs. 11.1 and 11.2). The first system is a nanoribbon fragment C_{130}, that is (9,6)-periacene, or shortly (9,6)-PA. Related structures are frequently considered in literature, particularly in the context of their polyradical character [8, 10]. Two other systems, GQD C_{130} and GQD C_{132}, belong to a class of recently synthesized colloidal graphene quantum dots [26] (see also Ref. [2]). For these GQDs, a simplified Hubbard-like π-electron model, with a somewhat artificial

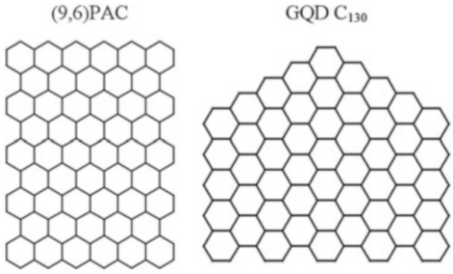

Fig. 11.1 Structure of the studied graphene molecules with strong and moderate electron correlation

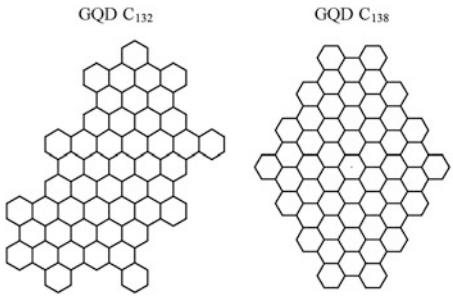

Fig. 11.2 Structure of the studied graphene molecules with weak electron correlation

Table 11.1 The π-electron RHF stability value λ^{stable}, lowest CIS excitation energy λ^{CIS}, and RAS-CI excitation energy $\lambda^{\text{RAS - CI}}$ (all values in eV) for singlet ($s = 0$) and triplet ($s = 1$) states in nanographenes

System	$\lambda^{\text{stable}}_{s=1}$	$\lambda^{\text{stable}}_{s=0}$	$\lambda^{\text{CIS}}_{s=1}$	$\lambda^{\text{CIS}}_{s=0}$	$\lambda^{\text{RAS-CI}}_{s=1}$	$\lambda^{\text{RAS-CI}}_{s=0}$
(9,6)-PA	−4.29	−0.35	−2.00	0.11	0.05	0.23
GQD C_{130}	−1.69	0.82	−0.17	1.15	0.14	0.75
GQD C_{132}	0.02	1.32	1.80	2.28	2.46	2.62
GQD C_{138}	−0.04	1.20	1.69	2.15	2.15	2.46

choice of π-parameters, was used in Ref. [2]. The last GQD C_{138} is the fully benzenoid (Clar's type) nanographene molecule, which should be particularly stable from the viewpoint of the so-called Clar aromatic sextet theory [14, 27].

Throughout the paper we apply the conventional Pariser-Parr-Pople π-electron Hamiltonian with the usual π-parameters (resonance integral $\beta_{CC} = -2.4$ eV, two-center Coulomb integrals $\gamma_{\mu\nu}$ due to Ohno, and one-center integral $\gamma_C = 11.13$ eV).

11.3.1 Hartree-Fock Instabilities and Optical Transitions

The key issue for large polycyclic hydrocarbons is their stability/instability as systems with spatially extended π-electron wave functions. The corresponding HF stability values along with CIS and RAS-CI results for excitation energies are listed in Table 11.1. The RHF stability and CIS excitations are studied here by using the conventional RHF MOs. As to our implementation of RAS-CI approach, we prefer, instead of RHF MOs, to utilize more sophisticated orbital sets such as in Ref. [28]. Only we used the EHF natural orbitals rather than the half-projected HF ones employed in [28].

From Table 11.1 we see that two first clusters, (9,6)-PA and GQD C_{130}, possess a strong triplet instability; furthermore, (9,6)-PA possesses, too, a clear singlet instability. It means that these π-structures cannot be correctly treated within RHF and related schemes. The erroneously negative value of $\lambda^{\text{CIS}}_{s=1}$ for GQD C_{130} in Table 11.1 is indicative of this point. At the same time, RAS-CI data (a penultimate column in

the table) show that all triplet excitation energies are positive, as it should be according to the known Ovchinnikov-Lieb rule for bipartite π-networks [29, 30]. The third system, GQD C_{132}, turns out to be a normal stable system with the lowest excitation energy in a visible optical region. The fully benzoid GQD C_{138} must absorb in the same optical region.

11.3.2 Effectively Unpaired Electrons

Firstly, we give some preliminary remarks. The effectively unpaired electron (EUE) theory provides a special understanding of strongly correlated spin-singlet systems in terms of loosely coupled electrons (for more detail see Ref. [8]). We only note that here we follow the Head-Gordon approach [31], but in fact the hole-particle analysis given in Ref. [6, 8] will be employed. In this approach, a special EUE number, N_{eff} (N_{U} in notation from Refs. [10, 31]), is constructed. In the hole-particle representation, N_{eff} is but a doubled occupation value of virtual particles, or explicitly,

$$N_{\text{eff}} = 2\sum_{a>n} \lambda_a,$$

with λ_a being the natural orbital occupation numbers for the particle (virtual) states of one electron. More exactly, $\{\lambda_a\}$ is understood as a set of the one-electron density matrix eigenvalues in a decreasing order. Within the EUE formalism, one can also introduce the associated EUE distribution $\left\{D^A_{\text{eff}}\right\}$ over all atoms $\{A\}$ [10, 31]. Furthermore, a suitable participation ratio index of the second order (PR2) serves to estimate an average number of the most active atoms on which unpaired electrons are localized; the PR2 precise definition is given in Ref. [8], Eq. (6.88). The above characteristics were employed in our investigation, and the main EUE results obtained at the EHF level are displayed in Fig. 11.3. In this figure the EUE

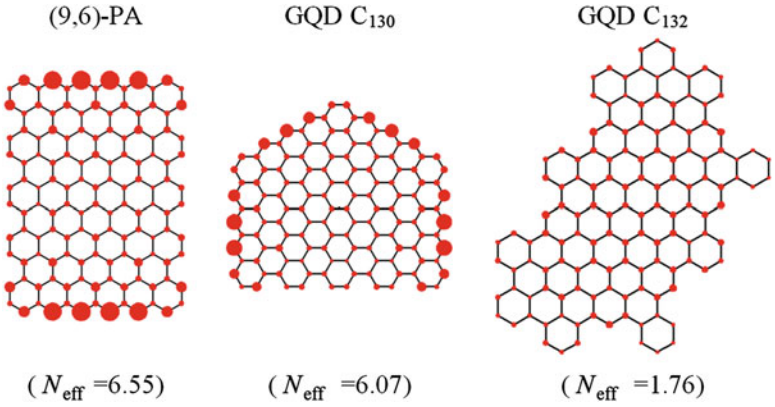

Fig. 11.3 EUE diagrams for the small graphene molecules treated by π-electron EHF method

distributions are visualized by diagrams in which atomic EUE densities are shown with red discs of radius proportional to the corresponding D_{eff}^{A} value. From the given diagrams, it follows that in case of the strongly correlated systems, that is, (9,6)-PA and GQD C_{130}, the number of unpaired electrons is significant ($N_{\text{eff}} \approx 6$), and they are localized on the zigzag (anthracene-like) part of the total board of the graphene structures. As in the previous studies [6, 8, 10], the armchair (phenanthrene-like) part of the board is almost not populated by unpaired electrons.

Opposite to (9,6)-PA and GQD C_{130}, the third system GQD C_{132} has a small $N_{\text{eff}} < 2$, and the corresponding EUE distribution is spread over the network more or less equally. These peculiarities in EUE localization are additionally reflected by the PR2 values (numbers of localization sites) which are rather small for the first two systems (PR2 = 13.8 and PR2 = 17.0, respectively) and too large for the last system (PR2 = 96.1). We do not display the EUE diagram for GQD C_{138} because in this molecule N_{eff} is too small ($\approx$0.36), so that the atomic EUE diagram becomes inexpressive ($D_{\text{eff}}^{A} \sim 10^{-3}$).

11.3.3 Characterizing Nanographene Aromaticity

It was long recognized that the aromaticity quantification is a too tricky matter. No wonder that there is a variety of quantum-chemical tools to understand aromaticity in a quantitative manner. Many such schemes are focused upon the so-called local aromaticity associated with a given benzenoid fragment in the whole system (e.g., see a fresh review [32] where one can find a vast literature on this issue).

In the present work, we apply a special aromaticity scale (σ_{arom} scale) proposed in Ref. [15]. It is based on comparing the atomization energies of the molecule under study and the related one produced by removing the given benzenoid ring A from the molecule. For the benzenoid cycle A, the corresponding local aromaticity index $\sigma_{\text{arom}}[A]$ is computed by Eqs. (73) and (74) in Ref. [15]. In Figs. 11.4 and 11.5, the local aromaticity diagrams are built from these $\sigma_{\text{arom}}[A]$ values which (in %) are inserted in benzenoid rings. The diagrams given here show, at the simple Hückel MO level, the typical features of distributing aromaticity over the graphene networks. To better understand them, it is useful to bear in mind an analogous image for the related hexacene molecule:

We see that in all structures, the most inner cycles are markedly less aromatic than the outer cycles. At the same time, the outer cycles belonging to a zigzag border of the nanographenes have also a lower aromaticity. We clearly observe that in all the systems, the armchair (phenanthrene-like) border regions show more aromatic, and thus more stable behavior. This fact is in conjunction to the EUE distributions given in Fig. 11.3.

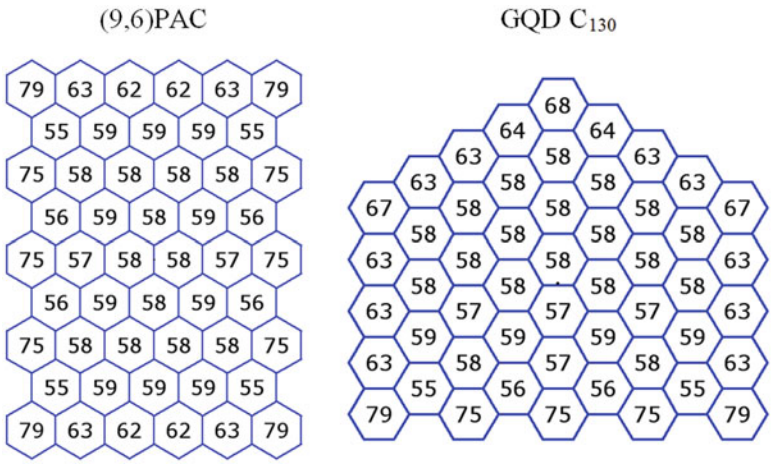

Fig. 11.4 Local aromaticity in the graphene molecules with strong and moderate electron correlation

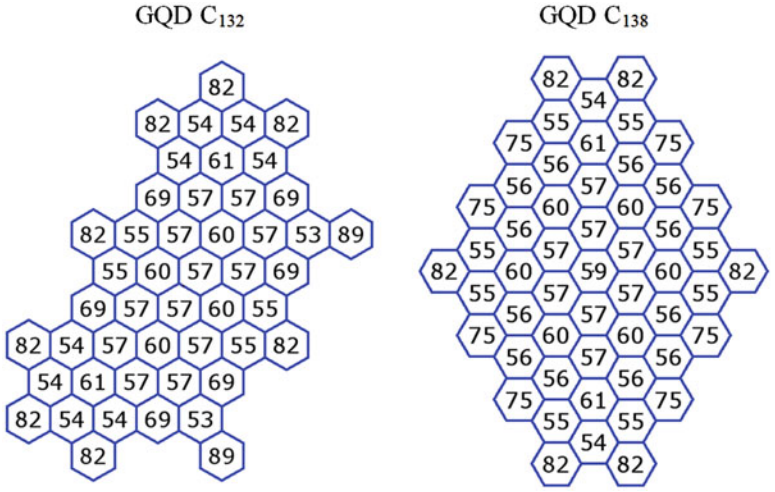

Fig. 11.5 Local aromaticity in the graphene molecules with weak electron correlation

11.3.4 Effects of Weak and Strong Electrostatic Fields

Over the last few years, there has been an upsurge of interest in the nonlinear optical properties (electric hyperpolarizabilities) of conjugated polymers and nanoclusters, including GQDs (see [33–36] and many others). In this subsection, we briefly examine the π-electron behavior of the nanographenes in presence of an electric field. The influence of electric fields, say, in *x*-direction, is usually modeled by

Table 11.2 Average π-electron polarizability and second-order hyperpolarizability (all in atomic units) for the graphene π-electron shells at the UHF level

Property	(9,6)-PA	GQD C_{130}	GQD C_{138}
α	1394	1366	1536
$\gamma \times 10^{-7}$	0.96	0.76	0.97

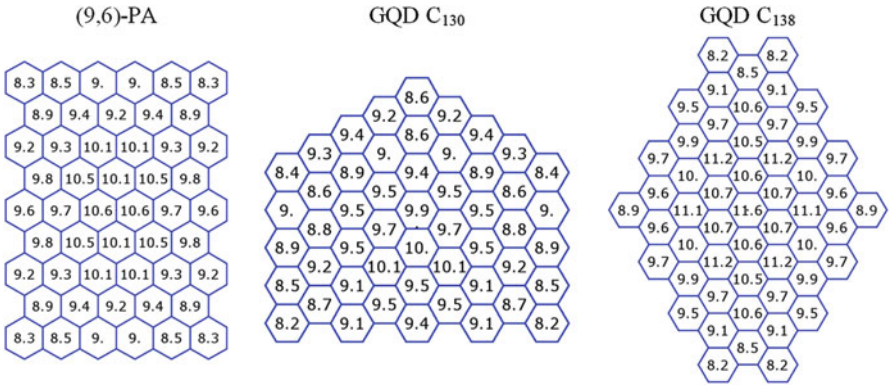

Fig. 11.6 Distribution of the average dipole π-polarizability in the small nanographenes at the UHF level

including in the full π-electron Hamiltonian the additional one-electron operator having atomic (μ,ν)-matrix elements proportional to $x_\mu\,\delta_{\mu\nu}$, with x_μ being x-coordinate of the μ-th atom. The proportionality constant is in fact a strength field F. Below in studying electric properties, we follow UHF approach rather than EHF, the latter requiring too much time to perform calculations repeatedly for many values of the field. Preliminary UHF and EHF computations on small acenes demonstrate reasonably similar field dependences of the main electronic properties. Our typical results for GQDs are presented in Table 11.2 and Fig. 11.6.

Before discussing them, recall that in weak electric fields, the key effect is well reflected through a small number of low-order electric polarizabilities. Namely, the molecular dipole moment induced by a small external electric field F is

$$d_{\text{ind}} \cong d + \alpha F + \beta F^2/2 + \gamma F^3/6,$$

where coefficients d, α, β, and γ are, respectively, the static dipole moment, (linear) polarizability, the first hyperpolarizability, and the second hyperpolarizability at the zero field. Besides, in the considered systems, which are all bipartite (alternant) ones, the dipole moment and the first hyperpolarizability are zero in standard π-electron approximations, so that $d_{\text{ind}} \cong \alpha F + \gamma F^3/6$.

The polarizabilities and hyperpolarizabilities were computed by the finite-field method (see, e.g., Ref. [37] for HF and Refs [35, 38] for FCI computations).

Table 11.2 displays the obtained α and γ data. We see that differences in the static electric properties of the molecules are not so significant. Concurrently, we must keep in mind that for the benzene (basic) molecule, the respective values are $\alpha = 25.3$ au and $\gamma = 788$ au. It means that an enormous exaltation of the static polarizabilities takes a place even in the case of small graphenes. For instance, GQD C_{138} formally contains only 23 benzene units C_6, whereas $\alpha[C_{138}]/\alpha[C_6] \cong 61$. In the case of hyperpolarizabilities, the tremendous nonadditivity effects make practically meaningless any comparison of the graphene γ values with that of the benzene subunit.

An additional interpretation of the above electric properties can be provided by their description in terms of local (atomic) contributions. Many theoretical (frequently rather sophisticated) procedures were proposed for dividing the total computed dipole polarizability into effective atomic polarizabilities $\{\alpha_\mu\}$ [39–42]. At the Hartree-Fock level, the simplest is the partition technique from Ref. [39], and below we will employ it. Only instead of the atomic contributions $\{\alpha_\mu\}$ including all atoms in the studied graphene structure, we make use of corresponding effective polarizabilities α_{Benzene} for each 6-atomic benzenoid cycle. These quantities are shown in the visible diagrams (Fig. 11.6) where numbers in hexagons are local effective α_{Benzene} values expressed in $A^\circ 3$. They should be compared with the reference magnitude $\alpha^0_{\text{Benzene}} = 3.8A^\circ 3$ of the isolated benzene. From Fig. 11.6 we observe that indeed the effective π-electron polarizabilities are essentially larger than $\alpha^0_{\text{Benzene}}$, and more importantly, they are markedly larger inside the graphene molecules than in peripheral hexagons. It means that in concordance with Figs. 11.4 and 11.5, in the nanographenes the aromaticity degree of inner cycles is lesser than that of border cycles. This is in line with a plausible suggestion that the aromaticity degree should be antibatic with the electronic polarizability. The assertion is supported by the so-called minimum polarizability principle [43] and its applications in many works, see, e.g., Refs. [44, 45].

To conclude the section, we shortly discuss the behavior of the same structures in strong fields. In Fig. 11.7 we show the field dependence of dipole moment d and the electron unpairing index N_{eff} (see Sect. 11.3.2). We observe in Fig. 11.7 a very large (sharp in certain field regions) increase of the dipole moment with applied field. Almost in the same field regions, N_{eff}exhibits sharp variations. Furthermore, under a very strong field, the great enhancement of radical character occurs, as it was previously reported for more simple conjugated molecules [8, 46]. The difference is that the external fields, which are causing polyradical-like structures in graphenes, are of an order of magnitude lesser as compared to those in Ref. [46]. It reflects an essentially increasing instability of nanographenes even in comparatively weak electric fields.

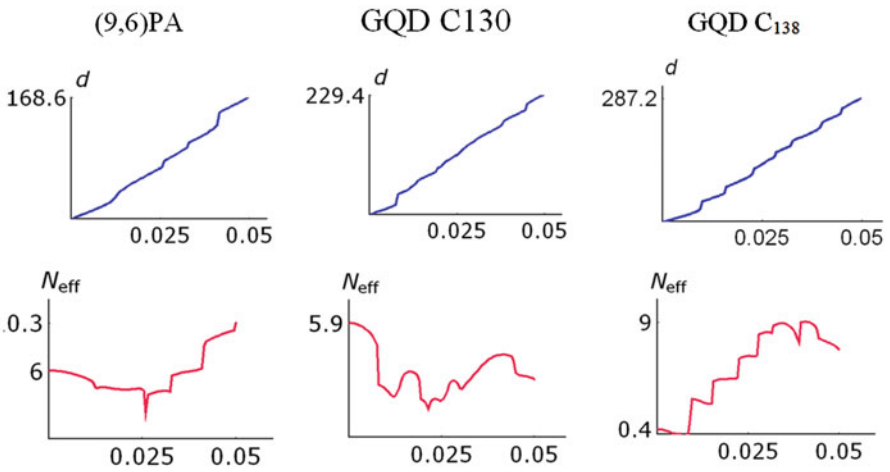

Fig. 11.7 Influence of strong electric fields on the nanographene dipole moment d (top) and effective electron unpairing N_{eff} (bottom) at the π-electron UHF level. The applied field (in atomic units) is in the long axis direction

11.4 Conclusion

We have studied the valence π-shells, i.e., the most active electron subshells, for several small graphene molecules. To this end, various approaches were employed, in each case depending on the solved problem and a feasibility of using the selected quantum chemistry method with the relatively modest hardware requirements. It was crucially important to take proper account of electron-correlation effects because many of them are found to exhibit a strong Hartree-Fock instability.

To obtain the lowest singlet and triplet excitations, we used the conventional RAS-CI technique with a special (EHF) orbital basis of natural states. The used CI technique guaranteed the non-negativity of computed triplet excitation energies $\lambda_{s=1}$ whereas the other well-known technique - CIS - did produce the wrong (negative) $\lambda_{s=1}$ in two GQDs where strong π-electron correlations take a place (Table 11.1).

Another important correlation effect is a large electron unpairing even in the ground singlet state of graphenes. The diagrams in Fig. 11.4 clearly demonstrate the unpairing effect for correlated π-systems of (9,6)-PA and GQD C_{130}. Moreover, an unusual behavior of the electron unpairing is observed in all GQDs when they are subjected to a sufficiently strong electric field. In that regard, the fully benzenoid structure GQD C_{138} turned out to be a remarkable example – a negligible initial (at the zero field) electron unpairing enormously increased even in moderate electric fields.

The last point which is worth discussing here is why we systematically use π-electron schemes whereas many authors follow seemingly more appropriate

DFT techniques. Indeed, DFT for not too huge clusters frequently gives good results (see Ref. [1] for DFT applications to graphenes). However, DFT is not an universal tool, saying nothing about a certain semiempirical character of energy functionals used in practical DFT calculations (a dependence on internal parameters of functionals, etc.). We do not also forget about a number of severe "ideological" difficulties in DFT (see review [47]), particularly those which are caused by absence of an explicit spin dependence in the general DFT theory (as McWeeny says, "unlike the classical position and momentum variables, electron spin is in a certain sense extraneous to the DFT." [48]; see also a careful analysis of Kaplan [49, 50]). In Ref. [51] one can find an interesting viewpoint on a special semiempirical use of the DFT technique as a possible tool for finding improved sets of π-electron parameters. We hope that in the future, our π-electron approaches to complex graphene networks can be further improved and extended with the help of more refined π-parameterizations [51].

References

1. Jiang DE, Chen Z (eds) (2013) Graphene chemistry: theoretical perspectives. Wiley, Puerto Rico
2. Güçlü AD, Potasz P, Korkusinski M, Hawrylak P (2014) Graphene quantum dots. Springer, Berlin/Heidelberg/New York
3. Kheirabadi N, Shafiekhani A, Fathipour M (2014) Review on graphene spintronic, new land for discovery. Superlattice Microst 74:123
4. Yin PT, Shah S, Chhowalla M, Lee K-B (2015) Design, synthesis, and characterization of graphene–nanoparticle hybrid materials for bioapplications. Chem Rev 115:2483
5. Georgakilas V, Perman JA, Tucek J, Zboril R (2015) Broad family of carbon nanoallotropes: classification, chemistry, and applications of fullerenes, carbon dots, nanotubes, graphene, nanodiamonds, and combined superstructures. Chem Rev 115:4744
6. Luzanov AV (2014) Measures of unpaired electrons for large conjugated systems. J Struct Chem 55:799
7. Luzanov AV (2014) Effectively unpaired electrons in bipartite lattices within the generalized tight-binding approximation: application to graphene nanoflakes. Funct Mater 21:414
8. Luzanov AV (2016) Effectively unpaired electrons for singlet states: from diatomics to graphene nanoclusters. In: Leszczynski J, Shukla MK (eds) Practical aspects of computational chemistry IV. Springer, Boston, p 151
9. Luzanov AV (2017) About theoretical peculiarities of lowest excitations in modified nanodiamond color centers. Funct Funct Mater 24:127
10. Luzanov AV, Plasser F, Das A, Lischka H (2017) Evaluation of the quasi correlated tight-binding (QCTB) model for describing polyradical character in polycyclic hydrocarbons. J Chem Phys 146:064106
11. Luzanov AV (2017) Localization of orbitals and electronic properties in nanodiamonds with color centers: semiempirical models. In: Fesenko O, Yatsenko L (eds) Nanophysics, nanomaterials, and applications, Springer proceedings in physics 195. Springer, Cham, p 115
12. Zdetsis AD, Economou EN (2015) A pedestrian approach to the aromaticity of graphene and nanographene: significance of Hückel's (4n+2)π electron rule. J Phys Chem C 119:16991
13. Saha B, Bhattacharyya PK (2016) Understanding reactivity, aromaticity and absorption spectra of carbon cluster mimic to graphene: a DFT study. RSC Advance 6:79768

14. Nishino N, Makino M, Aihara J-i (2016) Aromatic character of irregular-shaped nanographenes. J Phys Chem A 120:2431; Aihara J-i (2016) Graph theory of aromatic stabilization. Bull Chem Soc Jap 89:1425
15. Luzanov AV (2011) Quantum fidelity for analyzing atoms and fragments in molecule: APPLICATION to similarity, chirality, and aromaticity. Int J Quant Chem 111:2197
16. Čížek J, Paldus J (1967) Stability conditions for the solutions of the Hartree—Fock equations for atomic and molecular systems. Application to the pi-electron model of cyclic polyenes. J Chem Phys 47:3976
17. Helgaker T, Jorgensen P, Olsen J (2000) Molecular electronic-structure theory. Wiley, New York
18. Olsen J, Roos BO, Jorgensen P, HJAa J (1988) Determinant based configuration interaction algorithms for complete and restricted configuration interaction spaces. J Chem Phys 89:2185
19. McWeeny R (1992) Methods of molecular quantum mechanics. Academic Press, London
20. Koutecký J (1967) Unrestricted Hartree—Fock solutions for closed-shell molecules. J Chem Phys 46:2443
21. Löwdin P-O (1955) Quantum theory of many-particle systems. III. Extension of the Hartree-Fock scheme to include degenerate systems and correlation effects. Phys Rev 97:1505
22. Mayer I (1980) The spin-projected extended Hartree-Fock method. Adv Quant Chem 12:189
23. Mestechkin MM, Vaiman GE, Klimo V, Tino J (1983) Extended Hartree-Fock method and its application to molecules [in Russian]. Naukova Dumka, Kiev
24. Jiménez-Hoyos CA, Henderson TM, Tsuchimochi T, Scuseria GE (2012) Projected Hartree-Fock theory. J Chem Phys 136:164109
25. Luzanov AV, Ivanov VV (1991) Configuration interaction of states of the quasi-one-electron type. Theor Exp Chem 26:363
26. Yan X, Li B, Lim L-S (2013) Colloidal graphene quantum dots with well-defined structures. Acc Chem Res 46:2224
27. Clar E (1964) Polycyclic hydrocarbons. Academic Press, New York
28. Bofill JM, Pulay P (1989) The unrestricted natural orbital–complete active space (UNO–CAS) method: an inexpensive alternative to the complete active space–self-consistent-field (CAS–SCF) method. J Chem Phys 90:3637
29. Ovchinnikov AA (1978) Multiplicity of the ground state of large alternant organic molecules with conjugated bonds. Theor Chim Acta 47:297
30. Lieb EH (1989) Two theorems on the Hubbard model. Phys Rev Lett 62:1201
31. Head-Gordon M (2003) Characterizing unpaired electrons from the one-particle density matrix. Chem Phys Lett 372:508
32. Feixas F, Matito E, Poater J, Sola M (2015) Quantifying aromaticity with electron delocalisation measures. Chem Soc Rev 44:6434
33. Nagai H, Nakano M, Yoneda K, Kishi R, Takahashi H, Shimizu A, Kubo T, Kamada K, Ohta K, Botek E, Champagne B (2010) Signature of multiradical character in second hyperpolarizabilities of rectangular graphene nanoflakes. Chem Phys Lett 489:212
34. Nakano M, Champagne B (2016) Nonlinear optical properties in open-shell molecular systems. WIREs Comput Mol Sci 6:198
35. Zakharov AB, Ivanov VV, Adamowicz L (2016) Optical parameters of π-conjugated oligomer chains from the semiempirical local coupled-cluster theory. In: Leszczynski J, Shukla M (eds) Practical aspects of computational chemistry IV. Springer, Boston, p 57
36. Li H-P, Bi Z-T, Hu R-F, Han K, Li M-X, , Shen X-P, Wu Y-X (2017) Theoretical study on electronic polarizability and second hyperpolarizability of hexagonal graphene quantum dots: effects of size, substituent, and frequency. Carbon 122:756
37. Pople JA, McIver JW, Ostlund NS (1968) Self-consistent perturbation theory. I. Finite perturbation methods. J Chem Phys 49:2960
38. Pedash YF, Ivanov VV, Luzanov AV (1992) π-Electron hyperpolarizability of even-numbered polyenes in the complete configuration interaction method. Theor Exp Chem 28:19

39. Pedash VF, Luzanov AV (1981) Separation of the local contributions to the transition moments and the polarizability of a molecule in the self-consistent field method. J Struct Chem 21:439
40. Lazzeretti P, Zanasi R (1984) Resolution of molecular polarizability into atomic terms. Chem Phys Lett 109:89
41. Bader RFW (1990) Atoms in molecules – a quantum theory. Oxford University Press, Oxford
42. Otego N, Aslenoy CV, Pouchan C, Karamais P (2015) Hirshfeld-based intrinsic polarizability density representations as a tool to analyze molecular polarizability. J Comput Chem 36:1831
43. Chattaraj PK, Sengupta S (1996) Popular electronic structure principles in a dynamical context. J Phys Chem 100:16126
44. Chattaraj PK, Sarkar U, Roy DR (2007) Electronic structure principles and aromaticity. J Chem Educ 84:354
45. Santos JC, Contreras M, Merino G (2010) Structure and stability of Si 6 li 6: aromaticity vs polarizability. Chem Phys Lett 496:172
46. Luzanov AV (2013) π-system in a strong electric field. Analysis of electron unpairing. J Struct Chem 54:835
47. Kryachko ES, Ludeña EV (2014) Density functional theory: foundations reviewed. Phys Rep 544:123
48. McWeeny R (1994) Density functions and density functionals. Philos Mag B 69:727
49. Kaplan IG (2007) Problems in DFT with the total spin and degenerate states. Int J Quantum Chem 107:2595
50. Kaplan IG (2017) The Pauli exclusion principle: origin, verifications and applications. Wiley, Chichester
51. Chiappe G, Louis E, San-Fabián E, Vergés AV (2015) Can model Hamiltonians describe the electron-electron interaction in π-conjugated systems? PAH and graphene. J Phys Condens Matter 27:463001